Investigation into the Meshing Friction Heat Generation and Transient Thermal Characteristics of Spiral Bevel Gears

Yanzhong Wang[a], Wen Tang[a,*], Yanyan Chen[a], Tie Wang[b], Guoxing Li[b] , Andrew. D. Ball[c]

[a] School of Mechanical Engineering and Automation, Beihang University, Beijing, China.

[b] Department of Vehicle Engineering, Taiyuan University of Technology, Shanxi, China.

[c] School of Computing and Engineering, University of Huddersfield, UK

[*]Correspondence: E-mail: tangwen1205@163.com

Abstract

Friction loss and scuffing failure are two primary research subjects in improving the performance of spiral bevel gears. Aimed at improving the thermal characteristics with machine-setting parameter adjustment, a coupled thermo-elastic 3D finite element model has been developed to analyse the frictional heat generation and transient thermal behaviour of spiral bevel gears. The heat fluxes due to friction effects are applied to the gear tooth to investigate thermal characteristics and prediction of transient temperature fields. The resulting thermal characteristics agree with earlier work, thus verifying the model and numerical approach. This study permits an in-depth understanding of the temperature fields, together with the frictional heat generation process. Furthermore, by investigating the transient thermal behaviour among different pinion machine-setting parameters, the tilted and extended tooth contact pattern achieved by adjusting the machine-setting parameters can result in an optimal contact pattern that produces a uniform temperature field of much lower value, thereby achieving higher efficiency of transmission along with stronger anti-scuffing performance.

Key words: friction heat generation; transient thermal analysis; thermal-elastic coupled method; spiral bevel gear, tooth scuffing.

Highlights

A 3D FE method is established to analyse the friction heat generation of spiral bevel gears.

The distribution of the contact stress and heat flux on the tooth are evaluated.

Both the steady state and transient temperature fields have been explored.

The contact patterns have been obtained for better efficiency and anti-scuffing capacity.

1 Introduction

Spiral bevel and hypoid gears are widely used in major power transmissions including helicopter main gearboxes and vehicle differentials, and they face continuous demand for improvements in transmission reliability and efficiency. The efficiency of such gears is about 96% to 98% due to the high relative sliding experienced by the lubricated gear tooth contacts [1]. The tooth friction loss accounts for a considerable portion of gear transmission power losses, generating heat and leading to high local temperatures on contacting surfaces. Such significant local temperature rise is primary source of common surface failures such as micro-pitting, scoring and scuffing. Therefore, an in-depth understanding of frictional loss and flash temperature distribution is of significant importance for improving the efficiency and anti-scuffing capacity of spiral bevel and hypoid gears.

The heat generation of the gear meshing process is commonly considered as the main consequence of the friction loss. According to the flash temperature theory of Blok [2], the resultant heat flux between moving bodies was described as a product of friction coefficient,

applied pressure (load), and the relative velocity between the bodies [3]. In order to predict the friction power loss of hypoid gears, Kolivand and Kahraman [1, 5, 6] proposed an efficiency model which combines a computationally efficient contact model and a mixed elasto-hydrodynamic lubrication (EHL) based surface traction model. On this basis, Park [7] developed a hybrid contact model to predict the surface wear of hypoid gears.

Based on a unified mixed EHL model [8], Pu and Zhu [9] proposed a friction and flash temperature prediction approach for spiral bevel and hypoid gears and investigated the influence of surface velocity directions corresponding to different sliding velocities on the friction coefficient and flash temperature distribution in a wide range of speed and load. The EHL based model is capable of predicting the friction and flash temperature of the local meshing area. However, when it comes to the overall temperature field prediction of the gear tooth, finite element (FE) based thermal analysis is more effective as shown in 1995, Handschuh and Kicher [3] developed a FE based solution to predict the steady state and transient temperature fields of spiral bevel gears. In the study, an estimation of the heat flux magnitude and the location on the FE model was made according to the location, curvatures, orientations, and surface velocities of the tooth surface attainted by loaded tooth contact analysis (LTCA) of the spiral bevel gear. As a FE method allows tooth bending, contact deformation and load sharing between gear tooth pairs to be taken into account altogether, Bibel [10], Litvin [11] and Argyris [12] investigated a loaded meshing process of spiral bevel gears using FE models. They developed an automated approach for FE model generation. By conducting a quasi-static FE analysis, the contact force, the bearing contact and the transmission error have been characterised in order to accurately evaluate the load capacity and dynamic characteristic of the spiral bevel gear. However, the friction heat generation

and thermal characteristics were not considered in their models.

Of particular interest, Taburdagitan and Akkok [13] carried out a 2D coupled thermo-elastic analysis to investigate the tooth surface temperature rise of spur gears. They considered not only the elastic deformation, load sharing between contacting tooth pairs but also the heat generation from the contact tooth pairs. As a result, the analysis is more realistic and effective. This work has demonstrated that the coupled thermo-elastic FE analysis allows the frictional heat to be evaluated realistically in respect to the sliding velocity, contact pressure and friction coefficient for each node in the contact area, leading to both the stress and temperature distributions simultaneously. Therefore, this approach can be extended to the thermal analysis of a spiral bevel gears.

In this paper, the meshing heat fluxes of a pair of spiral bevel gear have been investigated by performing a coupled thermo-elastic analysis. It takes into account the load sharing and heat generation between contacting tooth pairs. Moreover, a 3D (rather than 2D) FE model is employed to achieve more accurate results. The heat flux distribution on the tooth surface is acquired directly from the coupled thermo-elastic analysis results. The transient temperature field of the gear tooth is obtained by applying the heat flux distribution to the transient thermal FE analysis models. Based on this established analysis approach, optimal machine-setting parameters with better efficiency and resistance to scuffing have been explored by investigating the effects of contact patterns on the thermal characteristics of spiral bevel gears.

2 Modelling the frictional heat generation of tooth meshing process

Based on the flash heat generation mechanisms, the heat flux between the tooth surfaces is jointly determined by the friction coefficient, the applied load and the sliding velocity between the tooth surfaces under contact. Specifically, frictional heat flux Q generated on a meshing contact

point of a gear pair can be calculated by:

$$Q = \mu F_n V_s \tag{1}$$

where μ is the coefficient of friction, F_n is the contact load at the contact point, and V_s is the relative sliding speed of the gear pair at the contact point. Usually, the tooth contact force F_n can be found through a loaded tooth contact analysis (LTCA) which can give the contact force, the path of contact, the transmission errors and the bearing contact as a set of instantaneous contact ellipses [4].

However, V_s needs to be calculated based on the kinematics of the contact points on the tooth. The contact point on the pinion and gear are represented by a pinion surface position vector $\mathbf{r}^p$ and a gear surface position vector $\mathbf{r}^g$. The pinion surface velocity vector $\mathbf{v}^p$ and the gear surface velocity vector $\mathbf{v}^g$ are defined as shown in Eqs. (2-3). $\boldsymbol{\omega}^p$ and $\boldsymbol{\omega}^g$ are the angular velocity vectors of the pinion and gear respectively. The sliding velocity vector $\mathbf{v}^s$ is defined as per Eq. (4). As the sliding velocity along the normal vector $\mathbf{n}$ has no contribution to heat generation, the value of sliding velocity V_s can be derived from Eq. (5).

$$\mathbf{v}^p = \boldsymbol{\omega}^p \times \mathbf{r}^p \tag{2}$$

$$\mathbf{v}^g = \boldsymbol{\omega}^g \times \mathbf{r}^g \tag{3}$$

$$\mathbf{v}^s = \mathbf{v}^g - \mathbf{v}^p \tag{4}$$

$$V_s = \left| \mathbf{v}^s - \mathbf{v}^s \cdot \mathbf{n} \cdot \mathbf{n} \right| \tag{5}$$

The friction coefficient μ is determined by the lubrication condition of the contacting gear tooth. Spiral bevel gears usually work under mixed lubrication conditions. As a result of the asperity contacts, the shear traction exerted onto the contacting surfaces consists of the viscous shear within the fluid regions and the asperity traction in regions of metal-to-metal contact. In order to

determine the friction coefficient along the path of contact, Kolivand and Kahraman [1] developed a friction coefficient prediction model and an empirical formulation was derived by carrying out a large number of EHL analyses. Pu and Zhu [8] proposed a unified mixed EHL model considering the effect of arbitrary velocity vector, relative sliding velocity, and microscopic roughness in the contact zone for spiral bevel and hypoid gears. According to their analysis, the friction coefficient can be in the range from 0.03 to 0.12 depending on the lubrication conditions (which are further correlated with operating conditions, lubricating oils, surface finishing and tooth profiles). According to the typical working condition of the spiral bevel gears under study, a constant friction coefficient μ=0.05 is used in this paper to carry out the following thermal analysis, which has lower computational demand compared with using a friction coefficient which varies with mesh position.

Fig. shows the characteristics of frictional heat fluxes, which are calculated based on the contact force and sliding velocity of a typical spiral bevel gear pair. The geometry parameters and the operating conditions of the spiral bevel gear are specified in Table . It can be seen that the maximum heat release occurs around the contact points at specific angular positions, before and after the pitch cone, where the contact involves higher load and greater sliding.

3 Finite element modelling and numerical simulation

To obtain the stress and temperature distribution of the spiral bevel gear, a 3D coupled thermo-elastic FE model is developed in this section for the spiral bevel gear pair under investigation. Thermal characteristics of the gear are investigated under both steady state and transient operating conditions.

3.1 Finite element model of the spiral bevel gear pair

By utilising a similar finite element modelling scheme to the one presented by Litvin et al.[4], the FE meshes have been automatically built from the points generated on the tooth flanks without using CAD software. There are 20 nodes along the profile direction and 40 nodes along the lead direction of the tooth surface, resulting in a FE model with 37,920 elements for both the pinion and gear, as shown in Fig., and this has been proven to provide sufficient accuracy. Moreover, in order to model both the elastic and thermal deformations, an 8-node thermally coupled brick element (C3D8T) together with a coupled temperature-displacement analysis step have been adopted.

The boundary conditions of the model are defined in Fig.. The rotation central points of the pinion and gear are fixed to the inner side of the pinion and gear body respectively, and all six degrees of freedom of the central point are restricted except for the rotation about the gear rotational axes. The tooth surfaces in contact are defined as surface-to-surface contact interactions, with properties as defined in Table 3. The initial temperature of the model and environmental sink temperature are both set at 20°C.

Based on the material properties of the gears, as detailed in Table 2, a numerical analysis was carried out via two main steps: firstly, a small rotation angle is applied at the centre of the pinion to ensure that the gear pair are in contact with each other. Following that, the method sets the analysis time duration to be 0.015s which enables the gear pair to rotate for several mesh cycles at a speed of 104.7rad/s (or 1000rpm) in order to achieve a consistent result and to show dynamic changes in temperature and contact stress. The rated torque of 600Nm is applied to the gear to simulate the loaded operation conditions.

3.2 Coupled thermo-elastic analysis of a pair of spiral bevel gear

The coupled thermo-elastic finite element analysis was conducted using ABAQUS software. It resulted in the temperature (NT11) fields of the pinion and gear as shown in Fig.. The highest temperature of both the pinion and gear is only 26°C because the initial temperature of the analysis is room temperature (20°C) and the pinion rotates for only 90 degrees. The temperature distribution of the pinion agrees with measured results obtained using the infrared microscope detailed in [3], in that the highest temperature occurs at the addendum of the pinion and the dedendum of the gear. The temperature at the pitch cone is lower than at either the addendum or dedendum of the tooth, because the sliding velocity there is relatively low. This agreement with measurements shows that this coupled thermo-elastic finite element model is an informative and defensible approach.

Fig. presents the maximum contact stress and the heat flux distribution on the tooth surface of the driven gear during a tooth-pair mesh cycle, again predicted using the coupled thermo-elastic FEA model in ABAQUS for the slave surface (or convex side) of the gear. The heat flux distribution represents the maximum nodal heat flux on the tooth surface throughout the mesh cycle. The instantaneous heat flux on the tooth surface can be obtained by summing all the nodal heat fluxes on the tooth surface. The comparison of the heat flux calculated by the friction heat generation formula (Eq.1) and the coupled thermo-elastic FEA model is shown in Fig.5. The average values of the friction heat flux obtained from the formula in Eq.(1) and the FEM are 31.3W and 171.8W respectively. This large temperature difference shows that the friction heat generation formula produces a less realistic result as it is calculated based on the instantaneous friction heat flux at the contact load and the relative sliding speed of a particular point, whereas

the coupled thermo-elastic FEA model produces the heat value accumulated across all the contacting nodes.

3.3 Steady state thermal analysis of a single gear tooth

In order to reach thermal steady state, when starting at room temperature, the simulation needs to repeat many thousands of iterations. Given the high computational demand of such repetitive simulation, it is not practical to predict the steady state temperature field for the whole spiral bevel gear with a comprehensive implementation of the coupled thermo-elastic analysis method. However, as the heat flux on the nodes can be obtained from the coupled thermo-elastic FEA results, a heat accumulated one tooth mesh modelling approach was implemented to obtain steady state thermal results. During this procedure, the heat flux is assumed to be of constant magnitude for each revolution of the gear. Since the heat flux distribution obtained from the coupled thermo-elastic FEA varies incrementally with time, the time-averaged constant heat flux Q_a on each node of the tooth surface can be calculated based on the heat of each node Q_n via

$$Q_a = \frac{\sum_{n=1}^{N} Q_n \cdot \left(\frac{t_m}{N} \right)}{t} \tag{6}$$

where N is the number of time step increments of the heat flux, t_m is the duration of the heat flux, and t is the total time of a gear rotation revolution. Subsequently, the time-averaged heat flux on each node calculated by Eq. (6) can be applied to the single tooth FEA model as the equivalent heat generated in the tooth meshing process. The 8-node linear heat transfer brick element (DC3D8) was used in the steady state thermal analysis model, along with the single tooth model shown in Fig.6 (which consists of 7,680 elements). In addition, considering the lubrication condition and the rotational speed of the gear, an assumption of air-oil mixed lubrication

convective boundary condition was made, in the same manner as Handschuh [3]. The heat transfer convection coefficients (h in $J/m^2 \cdot s \cdot K$) at the different boundary surfaces are specified in Fig. 7; it can be seen that the values at the tooth surfaces are higher than those of internal parts.

3.4 Transient thermal analysis of a single gear tooth

Likewise, for reasons of computational efficiency, the transient temperature field analysis was performed by assuming a steady state temperature field of the gear to be the initial condition. The time-varying heat flux distribution obtained from the coupled thermo-elastic FEA is applied to the tooth surface in a transient load step with a step interval of 0.015 seconds, to simulate the meshing friction heat generation process. A no-heat flux cycle is also applied for a time interval of 0.071 seconds to simulate the cooling process when the tooth is not in contact. The two load steps are repeated many dozen times to simulate the revolutions of the gear. The heat transfer convection coefficients at the boundary surfaces were taken as the same as for the steady state thermal analysis model in Fig. 7.

4 Results and discussion

4.1 Transient temperature field predicted by the coupled thermo-elastic model

The coupled thermo-elastic model is more advanced than the traditional finite element model because it considers the influence of friction heat generation and thermal deformation of the tooth. Further information, including the friction heat generation and the temperature field can be obtained from the coupled thermo-elastic analysis model. The transient thermal behaviour can be investigated in detail by comparing the temperature at three specified nodes: the addendum (node1), the pitch cone (node2) and the dedendum (node3) of the gear tooth, as depicted in Fig.8.

Fig.9 reveals that the temperature at node1 and node3 increases dramatically at the contacting position along with the accumulation of instant heat flux generated by friction. The temperature at node2 increases slowly because the friction heat at the pitch cone is relatively small due to the low sliding velocity at this location. However, with time there is a clear temperature rise at node2 and this is due to the effect of the heat conduction from other parts of the tooth such as node1. The temperature at node3 decreases immediately after contact, but increases again later as a consequence of heat conduction from the dedendum of tooth.

4.2 Transient temperature field predicted by steady state and transient thermal analysis model

As shown in Fig.10, the steady state temperature field of the driven gear tooth has been predicted based on the established steady state thermal analysis model and this is taken as the initial condition for the transient thermal analysis. The steady state thermal analysis simulates the continual rotation of the gear until thermal equilibrium is achieved, and the highest temperature of the steady state simulation is approximiately 105°C. As shown in Fig., the temperature field varies with the applied heat flux, with the highest temperature area located at the dedendum of the tooth. The temperature variations of the 3 nodes defined in the previous section are shown in Fig.. The temperature increases significantly (up to 112℃) as a result of the meshing friction heat flux and then decreases to a steady state (of about 104℃) in the following cooling cycle. The periodic fluctuation of the transient temperature curve demonstrates that the numerical simulation is already in steady state.

4.3 Effect of pinion machine-setting parameters on the thermal characteristics of the spiral bevel gears

The contact stress distribution, the sliding velocity and the friction coefficient, all of which have decisive influences on the meshing friction heat generation, can be affected by the contact patch shape and size. The contact patch can further be affected by the geometry of the mating gear or assembly error. In this paper, the machine-setting parameters (face-milling) which control the geometry of the pinion tooth surface, are considered as the main influencing factor of the contact pattern and have been investigated as a means of attaining lower heat generation and more uniform temperature fields. A case study has been conducted based on different machine-setting parameters to distinguish which form of contact patch is more suitable for improved efficiency and anti-scuffing performance. Table 4 presents three cases of machine-setting parameters associated with the pinion, which were found to be representative for defining an optimal contact pattern based on the studies of their temperature fields.

4.3.1 The characteristics of frictional heat fluxes

The loaded contact patch patterns of the driven gear, with different machine-setting parameters predicted by the classic LTCA approach, are shown in Fig.(a). Based on the theoretical friction heat generation model described in Section 2, the tooth contact force, the sliding velocity and the meshing friction heat fluxes are presented Fig. (b), (c) and (d) respectively, to reveal the effects of the three contact patterns. As the tilted angle between the contact point path and the root cone increases, the contact ratio increases in accordance because of the extension of the contact patch. This is illustrated by the increased length of the curved lines from Case 1 through Case 3 in Fig. 13 (a), in which Case 1 is taken as the baseline (the setting for the original design). The maximum load on the tooth and the sliding velocity at the same angle of gear rotation are both lower for Case 2 and Case 3 as shown in Fig. 13 (b) and (c), with Case 3 showing the largest change. These

improvements in turn make the maximum heat flux significantly lower, and the distribution of the heat flux more uniform, as shown in Fig. 13 (d). It can hence be concluded that the tilted and extended contact pattern has an obvious benefit to the reduction of frictional heat generation, which means that the transmission efficiency and anti-scuffing performance of Case 3 are likely enhanced.

4.3.2 The characteristics of the contact stress and heat flux distributions

With the evaluation conducted on all of the nodes of the tooth in the finite element model, the distributions of the contact stress and heat flux can be directly obtained from the FEA results. Fig. shows the loaded contact patterns (maximum contact stress distributions) predicted by the coupled thermo-elastic finite element model. The effect of pinion machine-setting parameters on the contact patterns are similar to the results predicted by the classic LTCA approach. The maximum value of the contact stress becomes lower with extension of the contact patch, resulting in a more uniform distribution of the contact stress on the tooth. The shape of the predicted contact pattern is a little different between the LTCA and the FEM because the FEM shows more detailed information about the contact, such as the stress concentration on the tip of the tooth and the change of contact area due to the change of tooth curvature.

The total heat flux distribution in one meshing cycle, as obtained from the coupled thermo-elastic FEA model, is shown in Fig.. Since the heat flux is evaluated according to the nodal stress, the sliding velocity, and the friction coefficient, the shape of the total heat flux distribution is similar to the distribution of contact stress. The total heat flux on the tooth surface is lower and more uniform as a result of the extension in the contact patch, and again the heat flux near the pitch cone is lower than the addendum and dedendum of the tooth because of the

relatively low sliding velocity.

4.3.3 The characteristics of transient temperature fields

The maximum temperature distribution on the tooth surface obtained from the transient thermal analysis is shown in Fig., in this figure the scales are different between three cases to highlight the differences of the temperature fields between them. Since the heat flux predicted by the coupled thremo-elastic model is the source of the temperature rise, the distribution of the temperature field on the tooth surface is similar to the heat flux. The temperature near the dedendum is the highest as a result of the high density of heat flux at the dedendum. Fig. shows the steady state temperature distribution on the tooth surface. With the extension of contact patchs across the three cases, the thermal radiation area on the tooth becomes larger and shifts towards to the toe of the tooth.

Fig. shows the transient temperature variations for the flash and bulk temperatures on the tooth for the three different pinion machine-setting parameters. It can be seen that the maximum value and extent of fluctuation of the flash temperature is the highest in Case 1 because of the relatively high density friction heat flux generated on the tooth surface in this case; in contrast, the flash and bulk temperatures in Case 3 are the lowest. It can again been seen that the tilted and extended contact pattern of Case 3 can likely outperform the other two cases in terms of anti-scuffing capacity and transmission efficiency.

5 Conclusions

Aimed at improving the thermal characteristics by adjustment of machine-setting parameters, a coupled thermo-elastic 3D finite element analysis has been performed to understand the meshing friction heat generation of a spiral bevel gear. The time-varying heat flux and its corresponding

distribution on the tooth surface have been attained, and the temperature fields of the gear tooth have been predicted by combined steady state and transient thermal analyese. Specifically, the highest temperature (at which scuffing is likely to start) is located at the addendum of the pinion and the dedendum of the gear. Furthermore, due to the relatively low sliding velocity, the highest temperature at the pitch cone is lower than that at either the addendum or dedendum of the tooth.

With these fundamental understanding of temperature distribution and the heat generation process, further study of three common pinion machine-setting configurations has revealed that a tilted and extended tooth contact patch pattern which produces the lowest temperature on the tooth surface; this in turn means the lowest heat generation and hence suggests an improvement in the efficiency and anti-scuffing capacity of the gears. The analysis approach developed in this paper can also be used to investigate the thermal behavior of other kinds of mechanical contacts such as those occurring in cylindrical and worm gears; this would provide reference for further topographical optimisation of the contact surfaces.

Acknowledgments

The authors are grateful for the financial support provided by the National Key Technology Research and Development Program (Grant No. 2014BAF08B01) of the Ministry of Science and Technology of China.

References

[1] M. Kolivand, S. Li, A. Kahraman, Prediction of mechanical gear mesh efficiency of hypoid gear pairs, Mechanism and Machine Theory, 45.11(2010):1568-1582. http://dx.doi.org/10.1016/j.mechmachtheory.2010.06.015

[2] H. Blok, Theoretical study of temperature rise at surfaces of actual contact under oiliness

lubricating conditions, Proc. Inst. Mech. Eng., 2 (1937): 222-235.

[3] R. Handschuh, Thermal behavior spiral bevel gears, NASATM-106518(1995). http://hdl.handle.net/2060/19950012520

[4] Litvin, F. L., and A. Fuentes, Gear Geometry and Applied Theory, Cambridge University Press, 2004.

[5] M. Kolivand, A. Kahraman, An Ease-Off Based Method for Loaded Tooth Contact Analysis of Hypoid Gears Having Local and Global Surface Deviations, Journal of Mechanical Design 132.7(2010):245-254. http://dx.doi.org/10.1115/1.4001722

[6] M. Kolivand, A. Kahraman, A load distribution model for hypoid gears using ease-off topography and shell theory, Mechanism and Machine Theory 44.10(2009):1848-1865. http://dx.doi.org/10.1016/j.mechmachtheory.2009.03.009

[7] D. Park, M. Kolivand, A. Kahraman, Prediction of surface wear of hypoid gears using a semi-analytical contact model, Mechanism and Machine Theory, 52 (2012) 180-194. http://dx.doi.org/10.1016/j.mechmachtheory.2012.01.019

[8] W. Pu, et al. A Theoretical Analysis of the Mixed Elastohydrodynamic Lubrication in Elliptical Contacts With an Arbitrary Entrainment Angle, Journal of Tribology 136.4(2014):410-419. http://dx.doi.org/10.1115/1.4028126

[9] W. Pu, J. Wang, D. Zhu, Friction and flash temperature prediction of mixed lubrication in elliptical contacts with arbitrary velocity vector, Tribology International 99(2016):38-46. http://dx.doi.org/10.1016/j.triboint.2016.03.017

[10] G. Bibel, R. Handschuh, Meshing of Spiral Bevel Gear set with 3D Finite Element Analysis, NASATM-107336 (1996).

[11] F. Litvin, et al. Computerized design, simulation of meshing, and contact and stress analysis of face-milled formate generated spiral bevel gears, Mechanism and Machine Theory 37.5(2002):441-459. http://dx.doi.org/10.1016/S0094-114X(01)00086-6

[12] J. Argyris, A. Fuentes, F. L. Litvin, Computerized integrated approach for design and stress

analysis of spiral bevel gears, Computer Methods in Applied Mechanics and Engineering 191.11-12(2002):1057-1095.
http://dx.doi.org/10.1016/S0045-7825(01)00316-4

[13] M. Taburdagitan, M. Akkok, Determination of surface temperature rise with thermo-elastic analysis of spur gears, Wear, 261.5-6(2006):656-665.
http://dx.doi.org/10.1016/j.wear.2006.01.019

[14] O. Vogel, A. Griewank, G. Bär, Direct gear tooth contact analysis for hypoid bevel gears, Computer Methods in Applied Mechanics and Engineering 191.36(2001):3965-3982.
http://dx.doi.org/10.1016/S0045-7825(02)00351-1

[15] V. Simon, FEM stress analysis in hypoid gears, Mechanism and Machine Theory 35.9(2000):1197-1220.
http://dx.doi.org/10.1016/S0094-114X(99)00071-3

[16] Y. P. Shih, A novel ease-off flank modification methodology for spiral bevel and hypoid gears, Mechanism and Machine Theory 45.8(2010):1108-1124.
http://dx.doi.org/10.1016/j.mechmachtheory.2010.03.010

[17] D. Park, A. Kahraman, A surface wear model for hypoid gear pairs, Wear 267.9–10(2009):1595-1604.
http://dx.doi.org/10.1016/j.wear.2009.06.017

[18] I. Karagiannis, S. Theodossiades, H. Rahnejat, On the dynamics of lubricated hypoid gears, Mechanism and Machine Theory 48.1(2012):94–120.
http://dx.doi.org/10.1016/j.mechmachtheory.2011.08.012

[19] E. Mermoz, et al. A new methodology to optimize spiral bevel gear topography, CIRP Annals - Manufacturing Technology 62.1(2013):119-122.
http://dx.doi.org/10.1016/j.cirp.2013.03.067

[20] W. Wang, et al. Deterministic solutions and thermal analysis for mixed lubrication in point contacts, Tribology International 40.4(2007):687-693.
http://dx.doi.org/10.1016/j.triboint.2005.11.002

[21] V. Simon. Influence of machine tool setting parameters on EHD lubrication in hypoid gears. Mechanism and Machine Theory 44.5(2009):923-937.

http://dx.doi.org/10.1016/j.mechmachtheory.2008.06.005

[22] Y. Shi, Y. P. Yao, J. Y. Fei, Analysis of bulk temperature field and flash temperature for locomotive traction gear, Applied Thermal Engineering 99(2016):528-536.
http://dx.doi.org/10.1016/j.applthermaleng.2016.01.093

[23] S. Li, A thermal tribo-dynamic mechanical power loss model for spur gear pairs, Tribology International 88(2015):170-178.
http://dx.doi.org/10.1016/j.triboint.2015.03.022

[24] G. Koffel, et al. Investigations on the power losses and thermal effects in gear transmissions, ARCHIVE Proceedings of the Institution of Mechanical Engineers Part J Journal of Engineering Tribology 1994-1996 (vols 208-210) 223.3(2009):469-479.
http://dx.doi.org/10.1243/13506501JET483

[25] E. Atan, On the prediction of the design criteria for modification of contact stresses due to thermal stresses in the gear mesh, Tribology International 38.3(2005):227-233.
http://dx.doi.org/10.1016/j.triboint.2004.08.005

[26] L. Bobach, et al. Thermal elastohydrodynamic simulation of involute spur gears incorporating mixed friction, Tribology International 48.48(2012):191-206.
http://dx.doi.org/10.1016/j.triboint.2011.11.025

[27] J. Xue, W. Li, C. Qin, The scuffing load capacity of involute spur gear systems based on dynamic loads and transient thermal elastohydrodynamic lubrication, Tribology International 79.79(2014):74-83.
http://dx.doi.org/10.1016/j.triboint.2014.05.024

[28] J. Zhang, et al. The effect of an oscillatory entrainment velocity on the film thickness in thermal EHL point contact, Tribology International 90(2015):519-532.
http://dx.doi.org/10.1016/j.triboint.2015.05.006

[29] R. Beilicke, L. Bobach, D. Bartel. Transient Thermal Elastohydrodynamic Simulation of a DLC Coated Helical Gear Pair Considering Limiting Shear Stress Behavior of the Lubricant, Tribology International 97(2016):136-150.
http://dx.doi.org/10.1016/j.triboint.2015.12.046

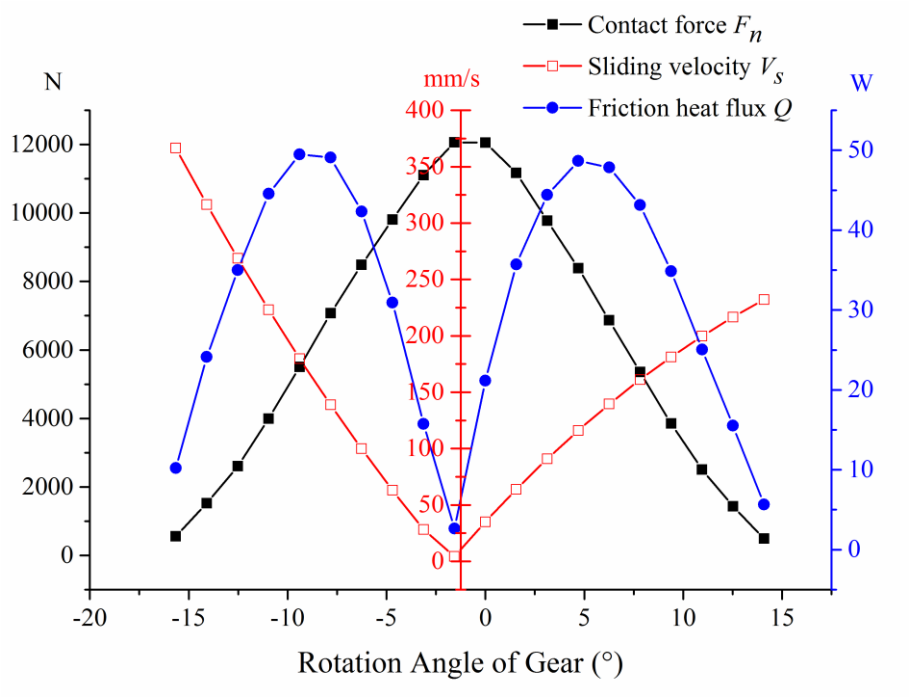

Fig. 1. The frictional heat flux of a spiral bevel gear pair versus contact load and sliding velocity.

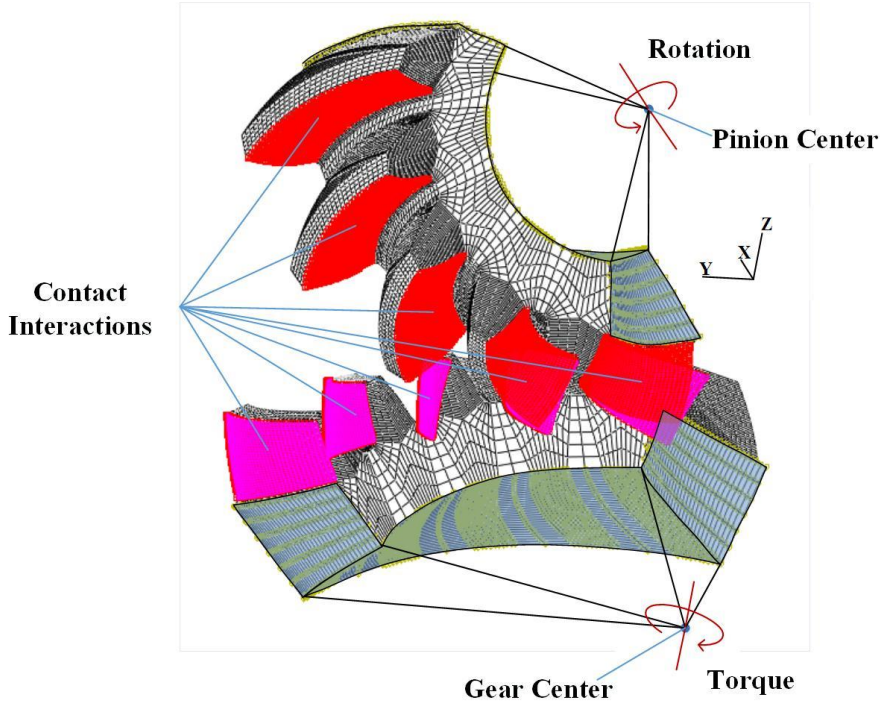

Fig. 2. The load and boundary conditions defined in the finite element model.

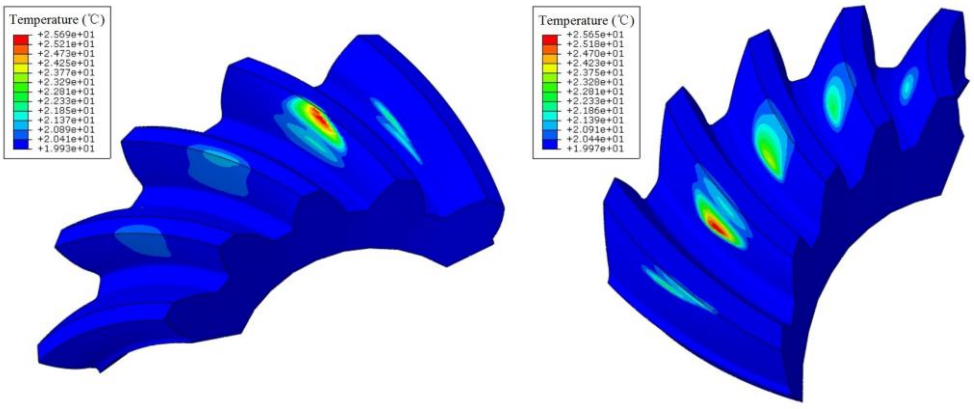

(a) Pinion (driving) (b) Gear (driven)

Fig. 3. Temperature field of the spiral bevel gear predicted by the coupled thermo-elastic model.

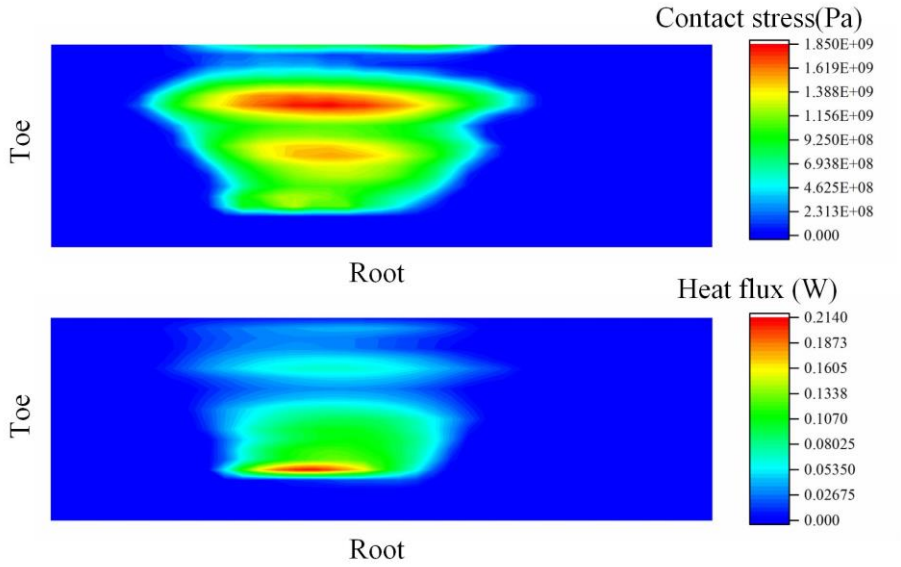

Fig. 4. Contact stress and heat flux distribution on the tooth surface of the driven gear.

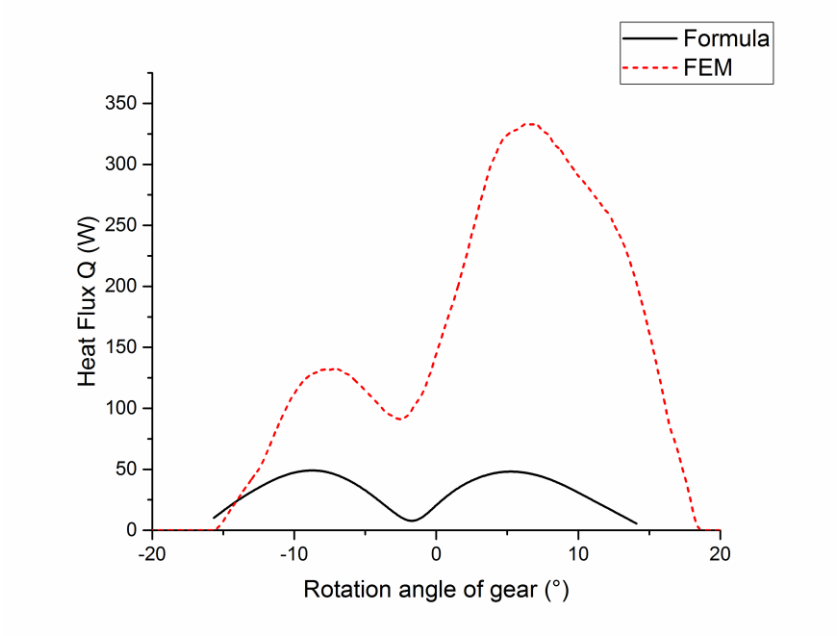

Fig. 5. The instantaneous heat flux obtained from the friction heat generation formula and the coupled thermo-elastic FEA model.

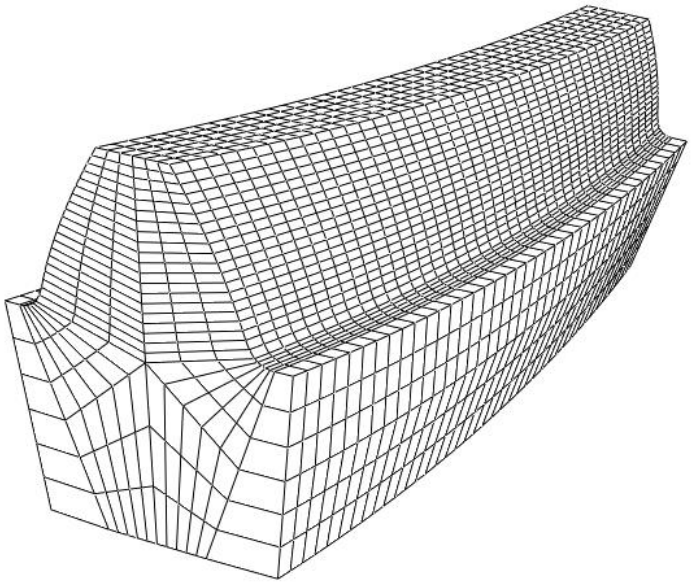

Fig. 6. Single tooth FE mesh model of the driven gear used in the thermal analysis.

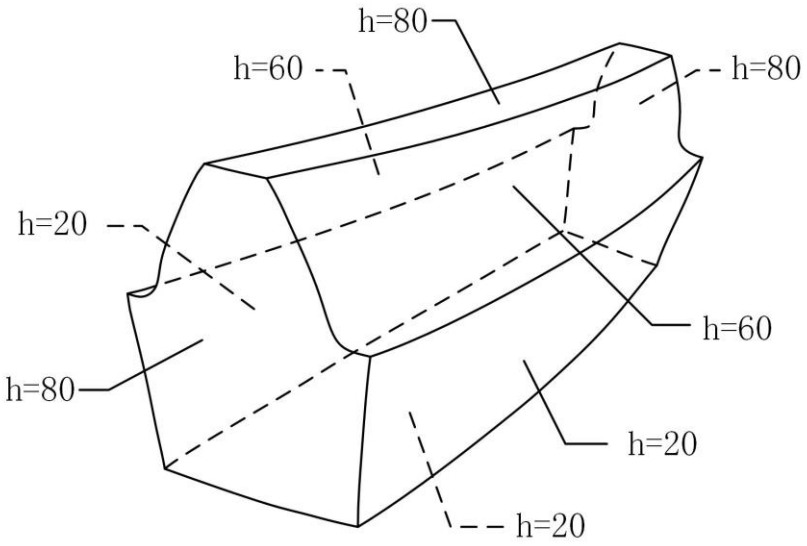

Fig. 7. Heat transfer convection coefficients to be specified for analysis.

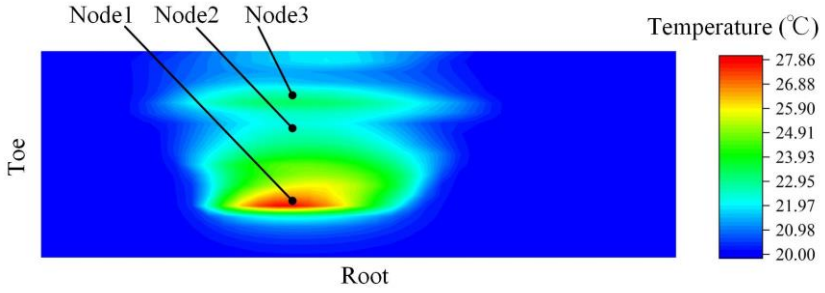

Fig. 8. Temperature distribution and positions of the specified nodes on the tooth surface of gear.

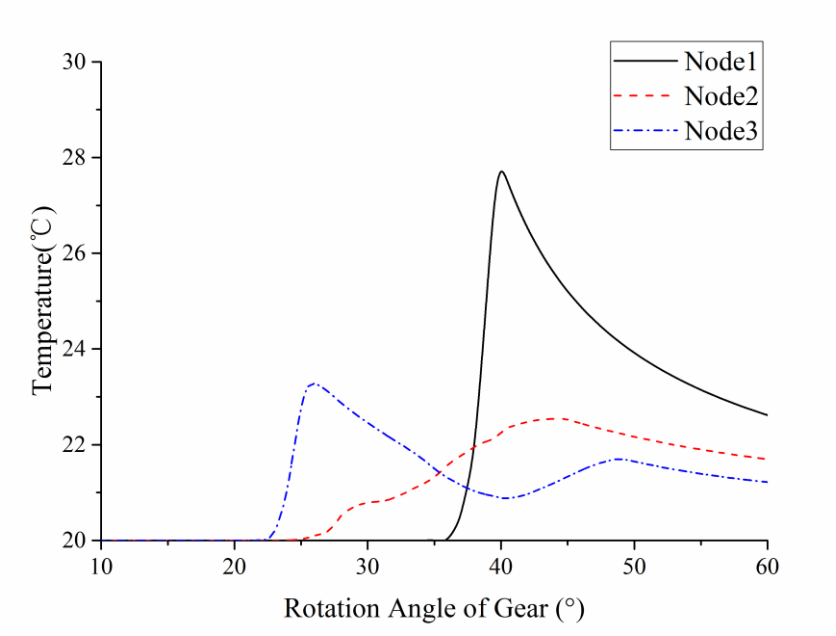

Fig. 9. Temperature variation at the specified representative nodes.

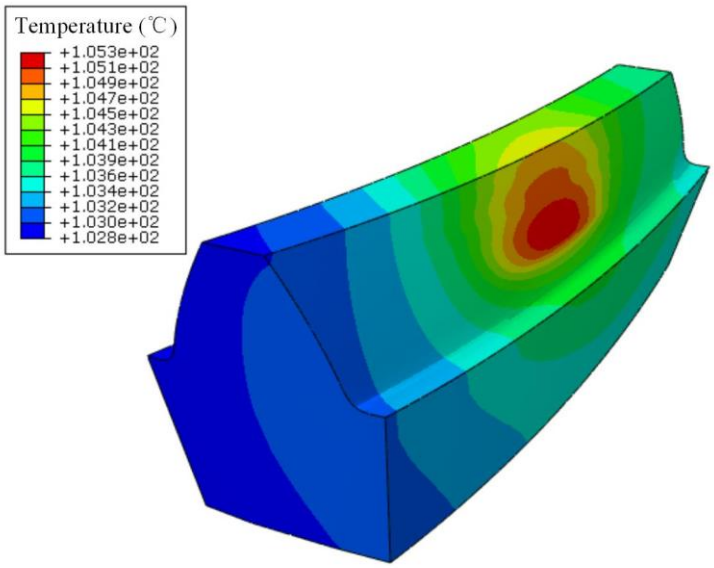

Fig. 10. Temperature field of the gear tooth in the steady state condition.

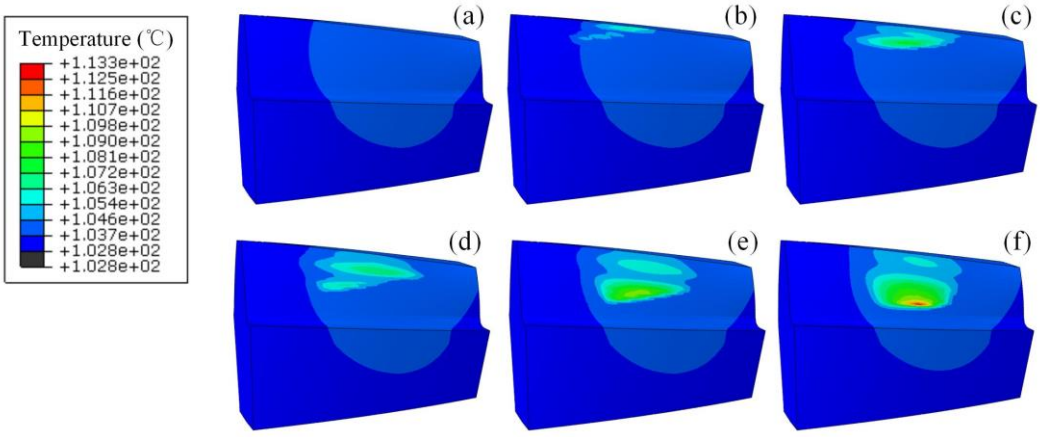

Fig. 11. Transient temperature field of the gear tooth in the meshing process: (a) initial condition; (b) start of the contact; (c) contact at the addendum; (d) contact at the pitch cone; (e) contact at the dedendum; (f) end of the contact.

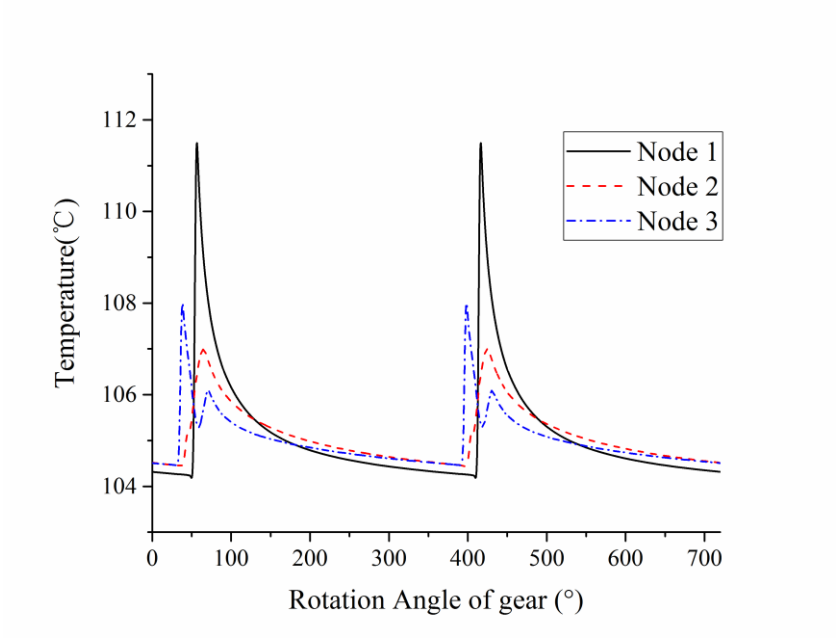

Fig. 12. Temperature variations of the specified nodes on the tooth surface.

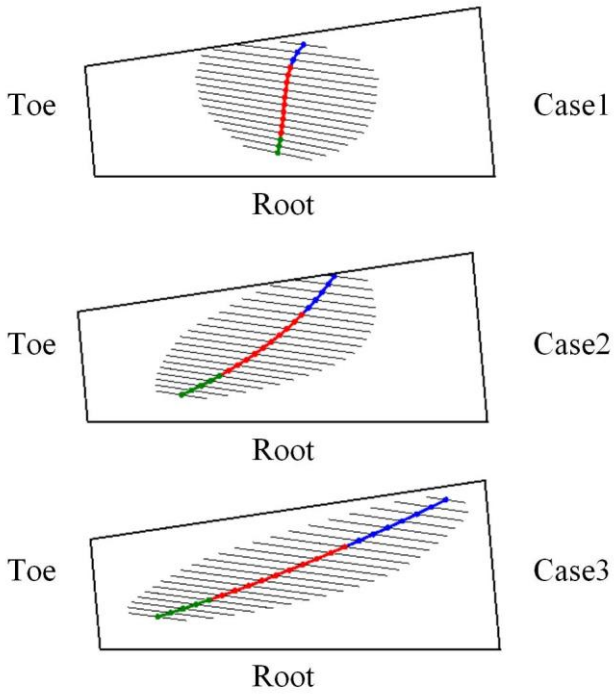

(a) Contact patchs

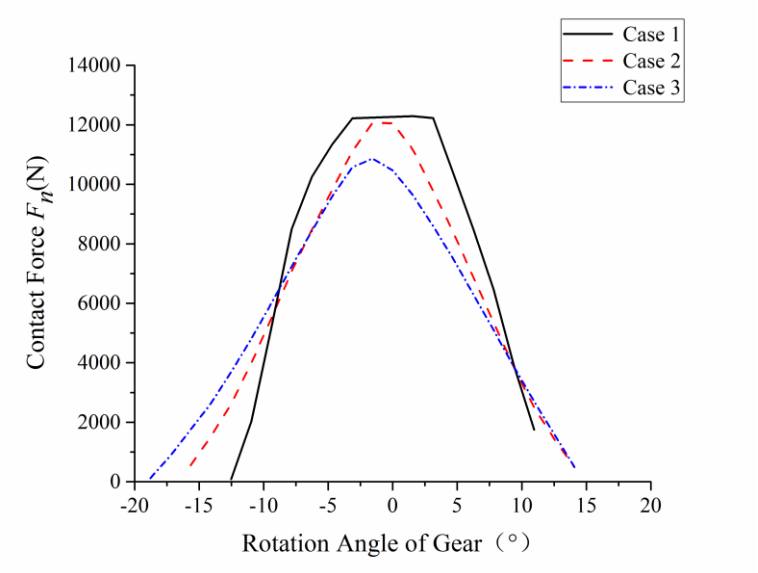

(b) Tooth contact force

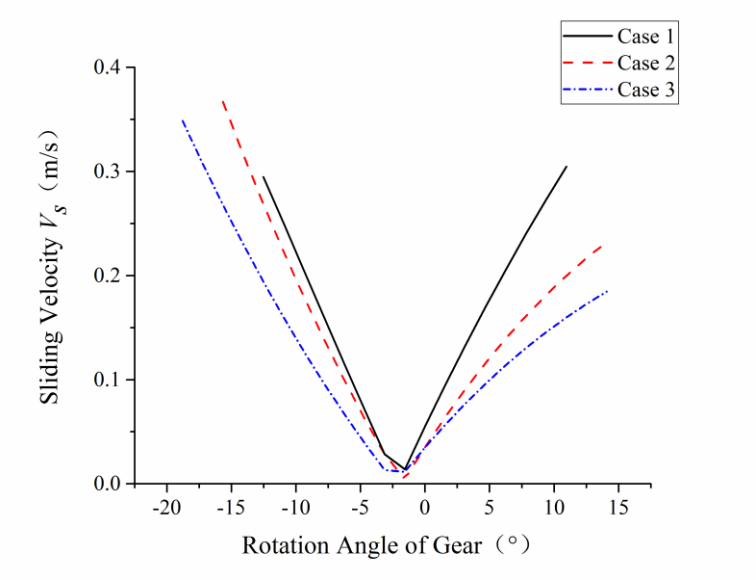

(c) Sliding velocity

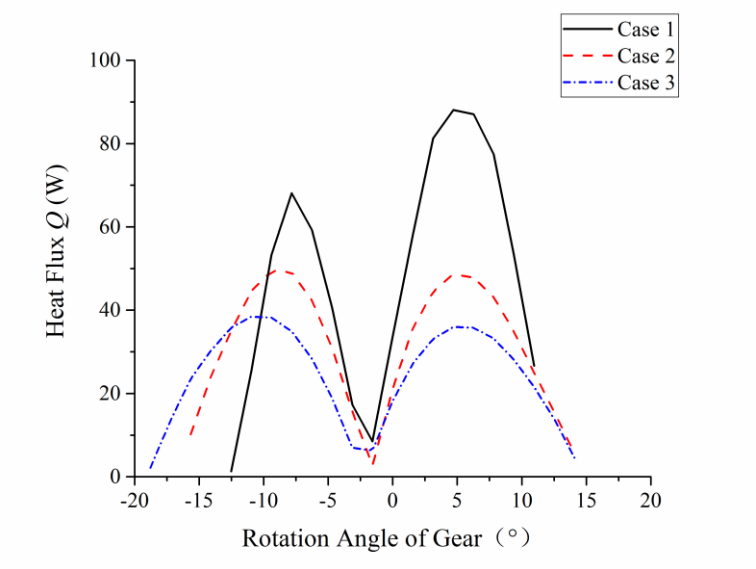

(d) Heat flux

Fig. 13. Friction heat flux for different pinion machine-setting parameters

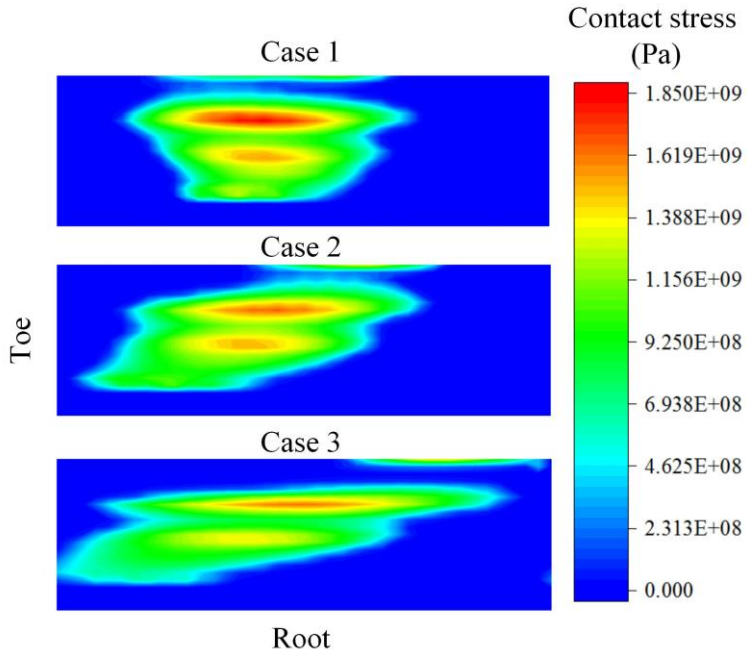

Fig. 14. Contact stress distribution with different pinion machine-setting parameters.

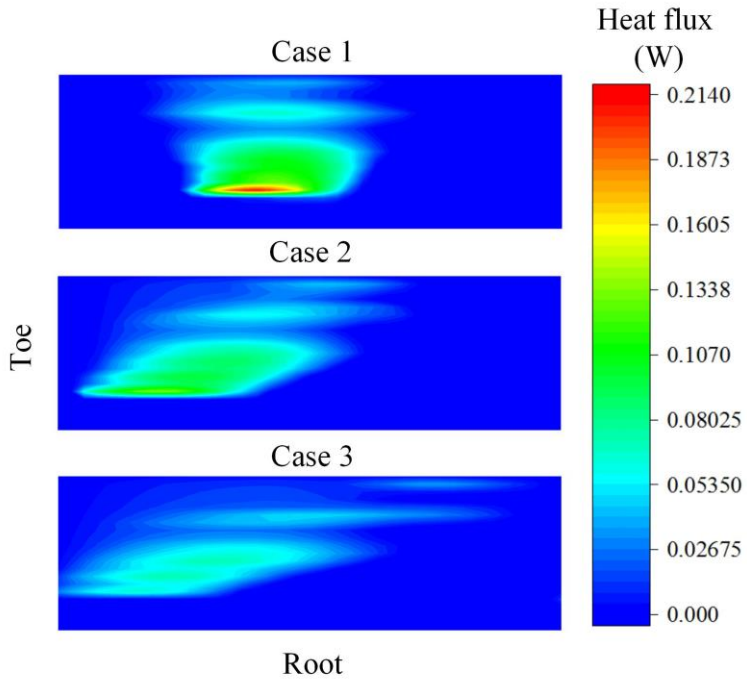

Fig. 15. Heat flux distribution with different pinion machine-setting parameters.

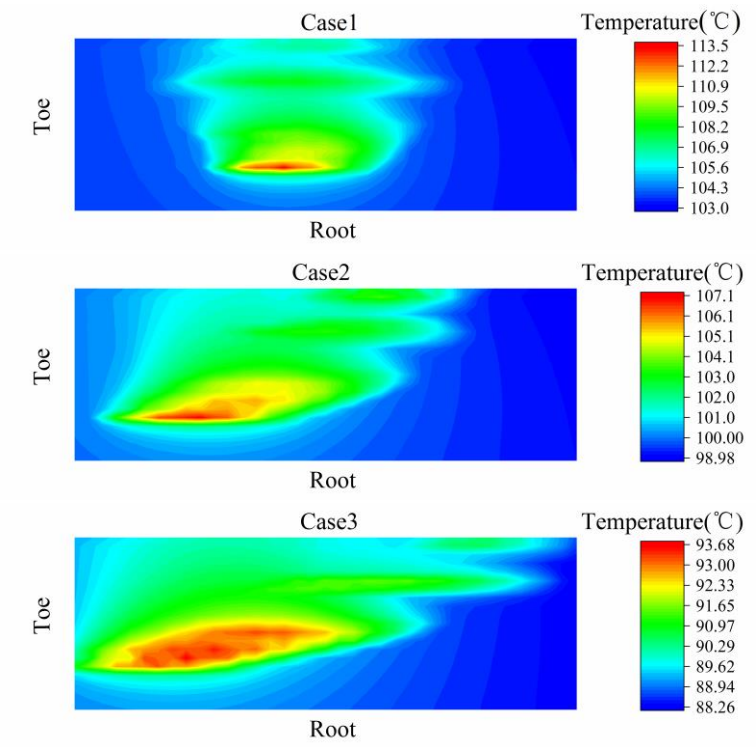

Fig. 16. The maximum temperature distribution on the tooth surface for different pinion machine-setting parameters.

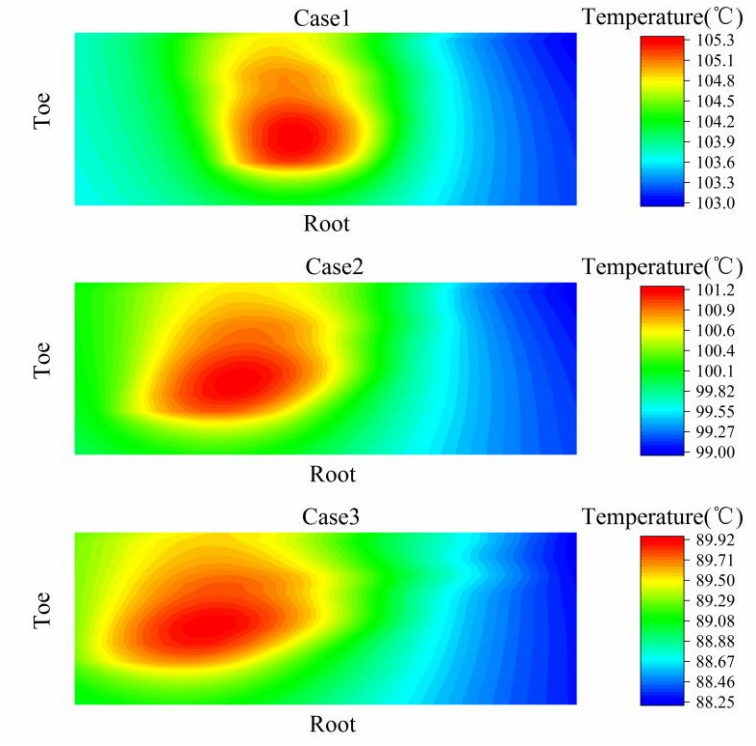

Fig. 17. Steady state temperature fields of the tooth surface for different pinion machine-setting parameters.

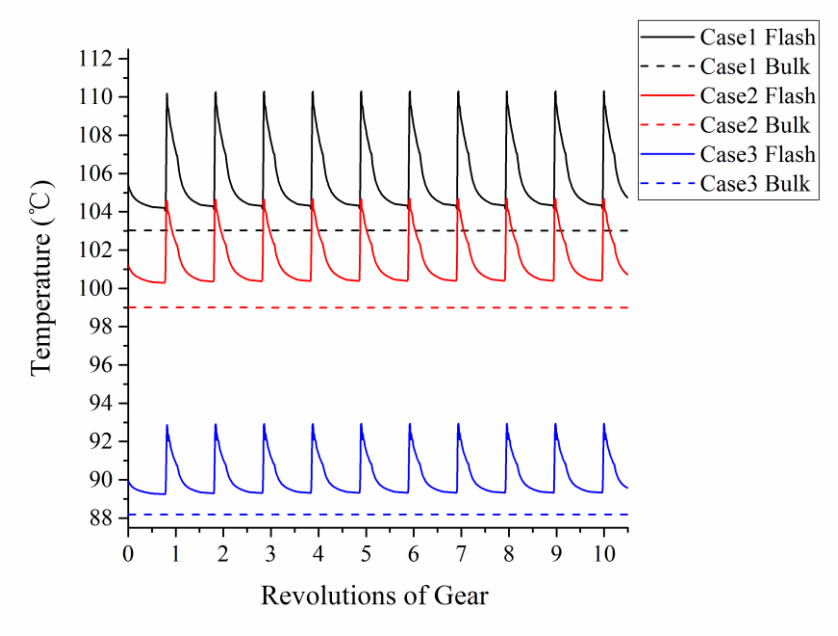

Fig. 18. Flash and bulk temperatures for different pinion machine-setting parameters.

Table 1. Geometry and working parameters of a typical spiral bevel gear pair.

	Pinion	Gear
Number of teeth	16	23
Module (mm)	6.522	
Outer pitch diameter (mm)	104.348	150
Face width (mm)	29	
Pitch angle (°)	34.8245	55.1755
Face angle (°)	39.8799	58.59364641
Root angle (°)	31.4064	50.1201
Outer cone distance (mm)	91.363	
Pressure angle at normal section (°)	20	
Mean helix angle (°)	35	
Shaft angle (°)	90	
Hand of spiral	Left hand	Right hand
Rotating speed(rpm)	1000	
Torque(N m)		600

Table 2. Material properties of the gear.

Elasticity Young's modulus (Pa)	2.1×10^{11}
Mass density (kg/m^3)	7.8×10^{3}
Thermal conductivity (J/m s K)	48
Coefficient of thermal expansion (1/K)	1.35×10^{-5}
Specific heat (J/kg K)	460

Table 3. Interaction properties of the contact surfaces.

Friction coefficient	0.05
Fraction of dissipated energy caused by friction that is converted to heat	1.0
Fraction of converted heat distributed to each surface	0.5

Table 4. Machine-setting parameters of the concave side of pinion.

	Case 1	Case 2	Case3
Cutter radius (mm)	70.358	71.755	70.993
Basic radial (mm)	58.534	69.520	67.948
Basic cradle angle (°)	65.739	64.667	63.497
Blank offset (mm)	-5.588	2.790	1.378
Machine centre to crossing point (mm)	-9.354	-1.914	-1.767
Sliding base (mm)	4.874	0.998	0.921
Ratio of roll	1.441	1.725	1.704